

Photoinduced complete melting of spin-Peierls phase in Na-tetracyanoquinodimethane revealed by frequency doubling of coherent molecular oscillations

H. Uemura, K. Iwasawa, H. Yamakawa, T. Miyamoto, H. Yada, and H. Okamoto

Department of Advanced Materials Science, University of Tokyo, Chiba 277-8561, Japan

(Received 12 June 2014; revised manuscript received 18 February 2015; published 5 March 2015)

Photoinduced melting of the spin-Peierls phase was investigated in Na-tetracyanoquinodimethane by pump-probe reflection spectroscopy with a time resolution of 49 fs. Photoirradiation generates coherent molecular oscillation, which indicates that the spin-Peierls dimerization decreased. Increasing the excitation photon density to > 0.02 photon/molecule doubles the oscillation frequency attributable to recovery of the original symmetry, that is, complete melting of the spin-Peierls phase. We observed a complete photoinduced transition with symmetry recovery revealed by frequency doubling of coherent oscillations.

DOI: [10.1103/PhysRevB.91.125111](https://doi.org/10.1103/PhysRevB.91.125111)

PACS number(s): 82.50.Hp, 78.20.-e, 78.40.Me, 78.47.jg

I. INTRODUCTION

Photoinduced phase transitions (PIPTs) in condensed matter are attracting much attention, not only as novel phenomena in solid-state physics but also as possible mechanisms for future optical switching and memory devices [1]. Correlated electron materials are good targets for PIPT studies because photoexcitation often triggers large changes in the electronic, magnetic, and crystal structures through strong interactions among the electrons (or charges), spins, and lattice degrees of freedom [2]. Photoinduced phase transitions in correlated electron materials are classified into two categories. The first includes purely electronic PIPTs represented by photoinduced Mott insulator-to-metal transitions observed in low-dimensional Mott insulators, such as a bromine-bridged Ni-chain compound $[[\text{Ni}(\text{chxn})_2\text{Br}]\text{Br}_2$: (chxn) = cyclohexanediamine] [3], an organic molecular compound, *bis*(ethylenedithio)tetrathiafulvalene-difluorotetracyanoquinodimethane (ET-F₂TCNQ) [4], and layered cuprates (Nd₂CuO₄ and La₂CuO₄) [5,6]. The second category consists of PIPTs accompanied by structural changes; characteristic examples are photoinduced insulator-to-metal transitions in VO₂ [7–11], perovskite manganites [12–16], and organic charge-order compounds [17,18]; photoinduced neutral-to-ionic phase transitions in tetrathiafulvalene-*p*-chloranil [19–24] and its derivatives [25]; and photoinduced melting of the charge-density-wave states in 1T-TaS₂ [26], TbTe₃ [27,28], and K_{0.3}MoO₃ [29]. In this category of PIPTs, lower symmetry structures are converted to higher symmetry ones by photoirradiation. In most of such PIPTs, the phase conversions are incomplete and part of the crystal is unchanged; that is, the recovery of the original higher symmetry is insufficient, although it is crucial in terms of both the physical mechanism and practical applications of PIPTs whether a complete photoconversion with symmetry recovery is achieved.

In this paper, we report an approach that discriminates photoinduced symmetry recovery using coherent oscillations of atoms or molecules generated in PIPTs. We study the photoinduced melting of the spin-Peierls phase [30–32] in Na-TCNQ [33]. In this compound, an electron is transferred from Na to TCNQ [Fig. 1(a)], and TCNQ[−] molecules are stacked along the *a* axis [Figs. 1(b) and 1(c)] [34,35]. Thus, a quasi-one-dimensional half-filled π electron band is formed along

the *a* axis. Because the on-site Coulomb repulsion U (~ 1.5 eV) of TCNQ is much larger than the transfer energy t (~ 0.2 eV) between two neighboring TCNQ molecules, this compound is a Mott insulator [33]. For $U \gg t$, a one-dimensional half-filled system can be regarded as an antiferromagnetic spin chain with $S = 1/2$. When the magnetic energy gain owing to singlet formation through lattice dimerization overcomes the lattice distortion energy, the lattice is dimerized. This transition is called a spin-Peierls transition [36]. Na-TCNQ shows lattice dimerization below 348 K [34,37] and is regarded as a spin-Peierls system [38,39].

Photoinduced melting of the spin-Peierls phase in Na-TCNQ was previously investigated by femtosecond pump-probe (PP) reflection spectroscopy with a time resolution of 180 fs [33]. Figure 1(d) shows the polarized reflectivity (R) spectrum along the *a* axis (broken line) and the previously reported photoinduced reflectivity changes (ΔR) after irradiation by a 130 fs laser pulse (1.55 eV) (open symbols). The peak at around 1 eV in the R spectrum corresponds to the Mott gap transition. Just after photoexcitation (0 ps), the spectral weight of the Mott gap transition was transferred below 0.5 eV, where midgap absorption was observed at ~ 0.3 eV, signaling polaron formation. After 1 ps, ΔR showed a characteristic peak at ~ 0.7 eV, and the ΔR spectrum was similar to the energy derivative of the original reflectivity (dR/dE) (lower panel), indicating a photoinduced decrease in the Mott gap transition energy E_g . In Na-TCNQ, E_g decreases with decreasing dimerization [33]. Thus, the ΔR spectrum after 1 ps itself indicates photoinduced melting of the spin-Peierls phase. In that paper, the dimeric molecular displacements after photoirradiation were evaluated to be $\sim 70\%$ of the original ones [33]. This suggests that a certain degree of dimerization remains, and a complete transition to a regular stacking structure was not realized. In that paper, coherent oscillations were also observed in the reflectivity changes ΔR , which were attributed to the release of the dimerization. However, the time resolution (180 fs) was not sufficient to fully reveal the ultrafast molecular dynamics.

Considering this background, here we report the photoinduced ultrafast molecular dynamics in Na-TCNQ investigated by PP reflection measurements with a time resolution of 49 fs. The excitation photon density dependence of the temporal evolution of ΔR revealed that the coherent oscillation frequency corresponding to the dimeric molecular displacements

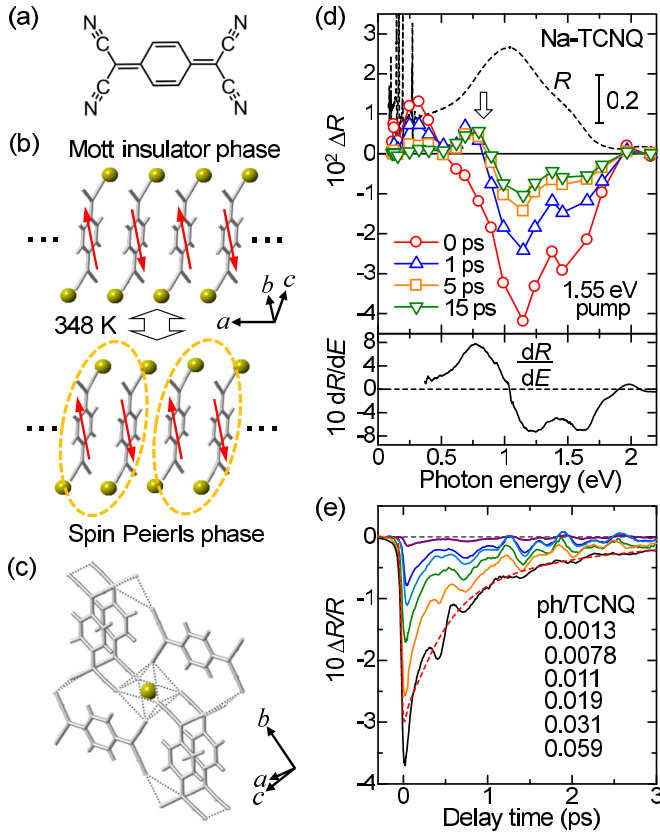


FIG. 1. (Color online) (a) Molecular structure of TCNQ. (b) Structures of TCNQ stacks in undimerized Mott insulator phase and dimerized spin-Peierls phase of Na-TCNQ. Spheres are Na⁺ ions. (c) Couplings between TCNQ stacks through Na ions. (d) Polarized reflectivity (R) spectrum (broken line) and photoinduced reflectivity change (ΔR) spectra (open symbols) measured with 180 fs time resolution [33]. Arrow indicates 0.83 eV. Solid line at bottom is dR/dE spectrum. (e) Temporal evolution of $\Delta R/R$ at 0.83 eV (1.97-eV pump) measured with 49 fs time resolution. Electric fields of pump and probe lights are parallel to the a axis. The broken line shows the background time profile for $x_{ph} = 0.059$ ph/TCNQ.

was doubled by strong excitation. We show that this frequency doubling is direct evidence of complete melting of the spin-Peierls phase and recovery of the original higher symmetry.

II. EXPERIMENTAL DETAILS

Single crystals of Na-TCNQ were grown by a diffusion method from NaI and TCNQ [37].

In the PP reflection measurement, we used a Ti : Al₂O₃ regenerative amplifier (photon energy: 1.56 eV, temporal width: 130 fs, and repetition rate: 1 kHz) as a light source. The output from the amplifier was divided into two beams. Both beams were used as excitation sources for two noncollinear optical parametric amplifiers, from which pump (1.97 eV) and probe (0.83 eV) pulses with a temporal width of 35 fs were obtained. The time resolution of the system is 49 fs. All the measurements were performed at 294 K.

By the Kramers-Kronig transformation of the polarized reflectivity (R) spectrum in Fig. 1(d), absorption depths of the pump (1.97 eV) and probe (0.83 eV) pulses were evaluated

to be 210 and 140 nm, respectively. So, measured reflectivity changes $\Delta R/R$ by the pump pulse reflect the photoinduced changes over the depth longer than 100 nm from the sample surface. The excitation photon density x_{ph} was defined as the photon density per unit volume within the absorption depth and evaluated using $x_{ph} = (1 - 1/e)(1 - R_p) \cdot I_p/l_p$, where I_p , l_p , R_p , and e are the excitation photon density per unit area, the absorption depth, the reflection loss of the pump light, and Napier's constant, respectively.

III. RESULTS AND DISCUSSION

Figure 1(e) shows the time characteristics of the photoinduced reflectivity changes ($\Delta R/R$) at 0.83 eV [the arrow in Fig. 1(d)] measured with 49 fs resolution for various excitation photon densities x_{ph} . $\Delta R/R$ at this energy sensitively reflects transient changes in the dimeric molecular displacements, as mentioned above. The decrease in the reflectivity just after photoirradiation is attributable to photocarrier generation. In K-TCNQ, which has almost the same structure and optical gap as those of Na-TCNQ, it was revealed that photocarriers were generated by photoirradiation above 1.5 eV [31]. We can consider that photocarriers are also generated by the 1.97 eV excitation in Na-TCNQ.

Subsequently, $\Delta R/R$ recovers with a time constant of ~ 0.5 ps. In the previous paper, the photocarrier decay time was evaluated as ~ 1.8 ps from the time characteristics of ΔR at 0.25 eV [33]. Thus, the subpicosecond recovery of $\Delta R/R$ in Fig. 1(e) is not due to photocarrier recombination, but indicates the presence of additional positive reflectivity changes, which can be related to the decrease in the dimerization, or equivalently the melting of the spin-Peierls phase, as discussed in the previous paper [33]. In addition, $\Delta R/R$ exhibits oscillatory structures.

To derive the oscillatory components, we subtract the background time profiles from the time evolutions of $\Delta R/R$. In this analysis, we assumed a function, $\sum_{i=1}^2 A_i e^{-t/\tau_i} + A_3 e^{-t/\tau_3} (1 - e^{-t/\tau_3}) + A_4 (1 - e^{-t/\tau_4})$, as background time profiles. The first, second, and third terms correspond to the bleaching, the melting of the spin-Peierls state, and the heating effect, respectively. To perform fitting procedures, this function was convolved with the Gaussian profile corresponding to the time resolution. As an example, the obtained background time profile for $x_{ph} = 0.059$ ph/TCNQ was shown by the broken line in Fig. 1(e). The parameter values used are $A_1 = -0.099$, $A_2 = -0.27$, $A_3 = 0.12$, $A_4 = 0.0068$, $\tau_1 = 2.0$ ps, $\tau_2 = 0.4$ ps, $\tau_3 = 0.1$ ps, $\tau_3' = 0.07$ ps, and $\tau_4' = 2.0$ ps. Figure 2(a) shows the excitation photon density dependence of the oscillatory components, $\Delta R_{osc}/R$, extracted by subtracting the background time profiles from $\Delta R/R$.

We tried to reproduce the oscillatory components for weak photoexcitation ($x_{ph} < 0.02$ ph/TCNQ) by using the following formula (the sum of three damping oscillators) with the least square method:

$$\frac{\Delta R_{osc}}{R} = \sum_{i=1}^3 -A_i \cos(\omega_i t + \phi_i) \exp\left(-\frac{t}{\tau_i}\right) \quad (A_i > 0). \quad (1)$$

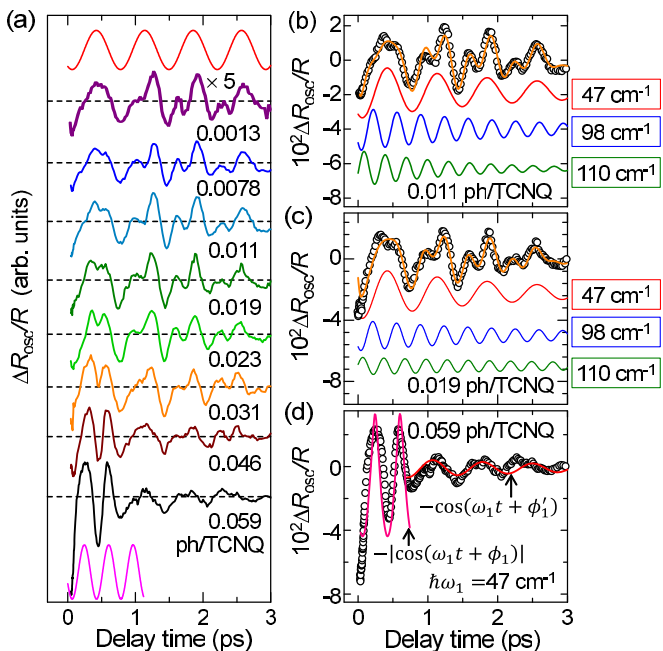


FIG. 2. (Color online) (a) Oscillatory components $\Delta R_{\text{osc}}/R$ of Na-TCNQ at 0.83 eV. Thin solid lines at top and bottom show 47 cm^{-1} and 93 cm^{-1} oscillations, respectively. (b, c) $\Delta R_{\text{osc}}/R$ (open circles) at 0.83 eV for (b) $x_{\text{ph}} = 0.011 \text{ ph/TCNQ}$ and (c) $x_{\text{ph}} = 0.019 \text{ ph/TCNQ}$. Orange lines show fitting curves. Three oscillatory components are shown in the lower part of each figure. (d) $\Delta R_{\text{osc}}/R$ (open circles) at 0.83 eV for $x_{\text{ph}} = 0.059 \text{ ph/TCNQ}$. Solid lines are proportional to $-\cos(\omega_1 t + \phi_1)$ and $-\cos(\omega_1 t + \phi'_1)$ ($\hbar\omega_1 = 47 \text{ cm}^{-1}$).

Figures 2(b) and 2(c) show the fitting results for $x_{\text{ph}} = 0.011$ and 0.019 ph/TCNQ , respectively, as typical examples, in which $\Delta R_{\text{osc}}/R$ is reproduced well, as shown by thick solid lines. The values of fitting parameters are given in Table I, in which error+ and error- show values of the upper limit and the lower limit of each parameter, respectively. Three components with $\hbar\omega_1 = 47 \text{ cm}^{-1}$, $\hbar\omega_2 = 98 \text{ cm}^{-1}$, and $\hbar\omega_3 = 110 \text{ cm}^{-1}$ are shown in the lower part of each figure. The initial phases ϕ_i for the former two modes ($i = 1$ and 2) are very small, so these oscillations are of the cosine type and are attributable to displacive excitation [40].

A previous Raman spectroscopic study revealed that the 47 cm^{-1} and 98 cm^{-1} modes correspond to dimeric molecular displacements along the stacking axis a and along the molecular planes, respectively [33]. At $t_d \sim 0.1 \text{ ps}$, the $\Delta R_{\text{osc}}/R$ components due to these two modes increase with time, indicating that the initial changes in the dimeric molecular displacements cause the blueshift of the Mott gap transition and correspond to photoinduced decreases in the degree of dimerization. In contrast, the 110 cm^{-1} mode is of the sine type, so it is attributable to impulsive stimulated Raman processes. The 47 cm^{-1} mode has the largest amplitudes. In fact, the oscillatory components up to 1 ps for $x_{\text{ph}} < 0.02 \text{ ph/TCNQ}$ almost coincide with the waveform of the 47 cm^{-1} mode [thin solid line at top of Fig. 2(a)]. On the other hand, when x_{ph} is increased above 0.02 ph/TCNQ , a dip appears at $\sim 0.4 \text{ ps}$ in $\Delta R_{\text{osc}}/R$, which is equal to a half-period of the 47 cm^{-1} mode. This dip structure becomes prominent as x_{ph} increases,

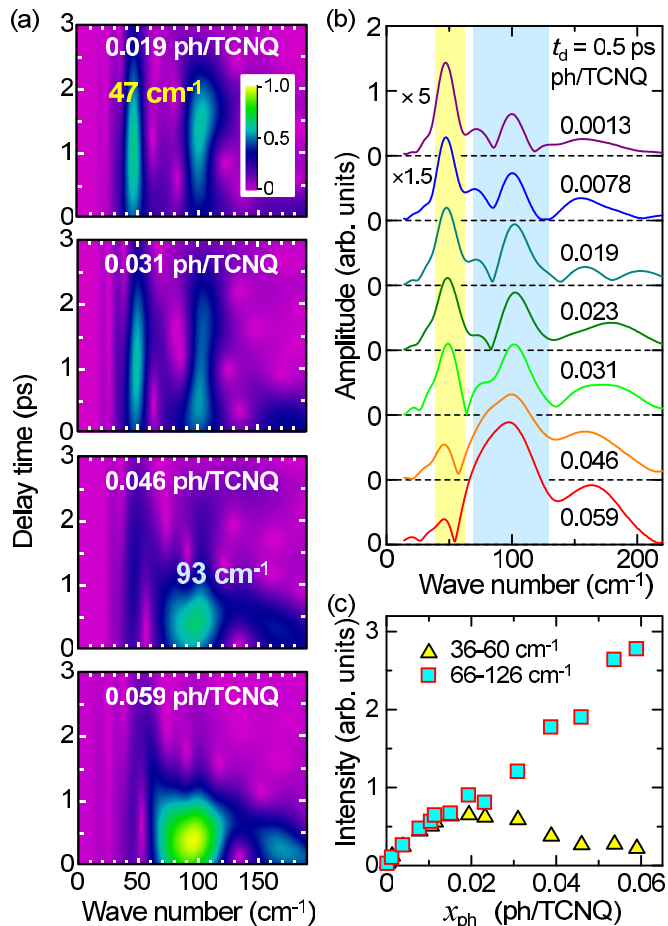


FIG. 3. (Color online) (a) Wavelet analyses of oscillatory components $\Delta R_{\text{osc}}/R$ at 0.83 eV in Na-TCNQ. (b) Fourier power spectra at 0.5 ps extracted from panel (a). (c) Intensities of 47 cm^{-1} and 93 cm^{-1} modes obtained by integrating the Fourier power spectra from 36 to 60 cm^{-1} and from 66 to 126 cm^{-1} , respectively. Integrated areas are indicated by colored shading in (b).

reminiscent of the 93 cm^{-1} oscillation. At 0.059 ph/TCNQ , the oscillatory component up to 1 ps is almost proportional to $-\cos(\omega t + \phi)$ with $\hbar\omega = 93 \text{ cm}^{-1}$ shown by the thin solid line at the bottom of Fig. 2(a) or $-|\cos(\omega_1 t + \phi_1)|$ with $\hbar\omega_1 = 47 \text{ cm}^{-1}$, as shown by the purple solid line in Fig. 2(d), which is the folded waveform of the 47 cm^{-1} oscillation [41]. After 1 ps, however, the 93 cm^{-1} mode disappears, and the mode with $\hbar\omega_1 = 47 \text{ cm}^{-1}$ [$-\cos(\omega_1 t + \phi'_1)$] reappears, as shown by the red solid line in Fig. 2(d) [42].

To see the time dependence of oscillatory profiles more clearly, we applied wavelet analyses [43] to $\Delta R_{\text{osc}}/R$ and obtained the time-dependent Fourier power spectra, which are shown in Fig. 3(a) as contour plots. For weak excitation ($x_{\text{ph}} < 0.02 \text{ ph/TCNQ}$), the 47 cm^{-1} mode is long-lived. The spectral weight at around 100 cm^{-1} can be seen only at $t_d > 0.5 \text{ ps}$. At $t_d < 0.5 \text{ ps}$, it is very small owing to the destructive interference of the 98 cm^{-1} and 110 cm^{-1} modes, as demonstrated by the fitting analyses in Figs. 2(b) and 2(c). When x_{ph} exceeds 0.03 ph/TCNQ , the 93 cm^{-1} mode becomes dominant at $t_d < 1 \text{ ps}$. For $x_{\text{ph}} = 0.059 \text{ ph/TCNQ}$, the spectral weight of the 47 cm^{-1} mode at $t_d < 1 \text{ ps}$ is negligibly small

TABLE I. Fitting parameters for the time characteristics shown in Figs. 2(b) and 2(c). Error+ and error- show values of upper limit and lower limit of each parameter, respectively.

x_{ph} [ph/TCNQ]		Amplitude A_i			Time constant τ_i [ps]			Wave number $\hbar\omega$ [cm^{-1}]			Phase ϕ_i [rad]		
		Value	Error +	Error -	Value	Error +	Error -	Value	Error +	Error -	Value	Error +	Error -
0.011	Mode 1	1.6E-02	1.9E-02	1.3E-02	2.6	2.8	2.2	46.6	47.3	45.7	2.6	2.8	2.4
	Mode 2	1.2E-02	1.5E-02	1.0E-02	2.3	2.6	1.7	98.0	100.4	95.8	2.3	2.7	2.0
	Mode 3	1.1E-02	1.4E-02	7.0E-03	1.4	2.0	1.1	110.2	114.9	107.5	4.5	5.0	4.1
0.019	Mode 1	1.7E-02	2.2E-02	1.5E-02	2.2	2.8	1.3	46.6	47.6	45.7	2.6	3.0	2.3
	Mode 2	1.0E-02	1.3E-02	7.0E-03	2.6	4.0	1.8	98.0	100.4	95.8	2.4	2.9	2.0
	Mode 3	5.8E-03	8.0E-03	3.0E-03	3.8	10.0	1.0	110.2	114.9	107.5	4.9	5.4	4.5

compared to that of the 93 cm^{-1} mode, whereas at $t_d > 1 \text{ ps}$, the 93 cm^{-1} mode almost disappears, and instead the 47 cm^{-1} mode is restored, as seen by the color change from bright purple to dark navy.

To obtain more quantitative information on the excitation photon density dependence of the 47 cm^{-1} and 93 cm^{-1} modes at $t_d < 1 \text{ ps}$, we extracted the Fourier power spectra at 0.5 ps for various x_{ph} values [Fig. 3(b)]. The spectral shapes are almost unchanged for $x_{\text{ph}} < 0.02 \text{ ph/TCNQ}$. Four structures appear: a strong peak at 47 cm^{-1} ; a medium-intensity peak at around 100 cm^{-1} , which consists of two oscillatory components at 98 cm^{-1} and 110 cm^{-1} [see Figs. 2(b) and 2(c)]; and two small peaks at 75 cm^{-1} and around 150 cm^{-1} , which were not considered in the fitting analyses in Fig. 2. The origins of the 75 cm^{-1} and 150 cm^{-1} oscillations are unclear at present. Fitting curves, which do not include these modes, almost reproduce the time characteristics of the oscillations [e.g., Figs. 2(b) and 2(c)], so that the intensities of these oscillations should be small.

For $x_{\text{ph}} = 0.046 \text{ ph/TCNQ}$, the intensity of the 47 cm^{-1} mode decreases considerably. Instead, a broad band appears at around 90 cm^{-1} and gains in intensity with increasing x_{ph} . Note that the center of the spectral weight of this band is $\sim 93 \text{ cm}^{-1}$, which differs from that of the peak (100 cm^{-1}) of the band observed for $x_{\text{ph}} < 0.02 \text{ ph/TCNQ}$. Figure 3(c) shows the spectral intensities at 0.5 ps integrated over $36\text{--}60 \text{ cm}^{-1}$ and $66\text{--}126 \text{ cm}^{-1}$ [shaded areas in Fig. 3(b)], which reflect the intensities of the 47 cm^{-1} and 93 cm^{-1} modes, respectively. The intensities in these two regions are almost proportional to x_{ph} up to $\sim 0.015 \text{ ph/TCNQ}$. At $x_{\text{ph}} > 0.02 \text{ ph/TCNQ}$, the intensity in the lower frequency region (47 cm^{-1} mode) decreases considerably, and the intensity in the high-frequency region (93 cm^{-1} mode) increases, showing frequency conversion from 47 to 93 cm^{-1} .

This frequency conversion can be explained as follows. For the weak excitation case, as shown in Fig. 4(a), the photoinduced melting of the spin-Peierls phase is incomplete, and dimerization remains; consequently, the phase ψ_{OSC} of the coherent oscillation $\Delta R_{\text{OSC}}/R$ is equal to the phase ψ of the molecular vibration [Figs. 4(a)(i)–(iii)]. Therefore, the reflectivity oscillates with the same frequency as the corresponding molecular vibration, ω_1 , in the spin-Peierls phase [Fig. 4(a)(iv)]. In contrast, for the strong excitation case, as shown in Fig. 4(b), the spin-Peierls phase is completely destabilized [Figs. 4(b)(i)–(iii)], so molecules oscillate around equally spaced positions [Fig. 4(b)(iv)], as in the

high temperature phase without dimerization. In this case, the molecular oscillation phases $\psi = 0$ and π yield two equivalent states characterized by the same ψ_{OSC} , which are dimerized in opposite directions [Figs. 4(b)(i) and (ii)] and gives the same optical responses as shown by the red line in Fig. 4(b)(iv), if the oscillation amplitude does not decay. As a result, $\Delta R_{\text{OSC}}/R$ oscillates with $2\omega_1$ [Fig. 4(b)(iv)]. For an intermediate-intensity excitation, both of the coherent oscillations with the frequencies ω and 2ω might be observed.

More strictly, $\Delta R_{\text{OSC}}/R$ under strong excitation differs slightly from that of a harmonic oscillator with $2\omega_1$ but

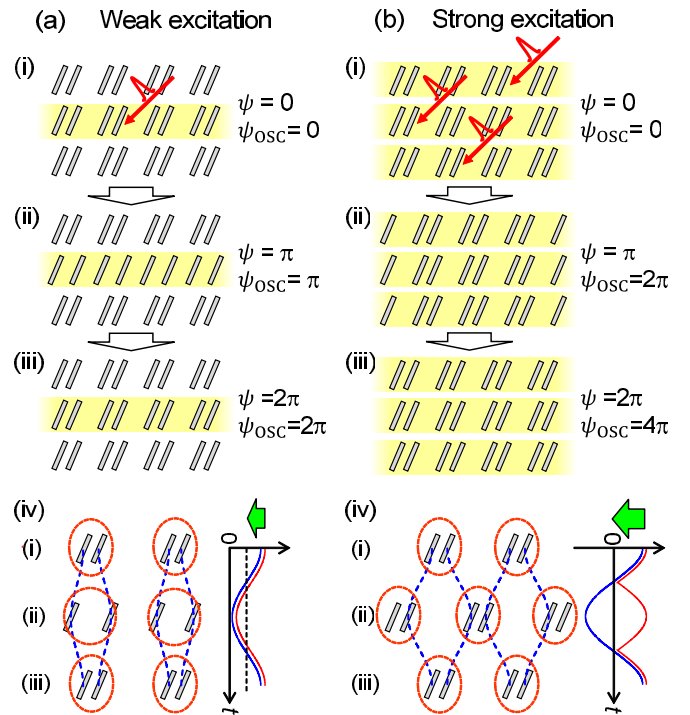


FIG. 4. (Color online) Schematics of transient changes in dimeric molecular displacements: (a) weak and (b) strong excitation cases. Figures (i)–(iii) show molecular configurations at typical times. ψ and ψ_{OSC} are the phases of the molecular oscillation and coherent oscillation $\Delta R_{\text{OSC}}/R$, respectively. (iv) Left: Time dependence of molecular configurations. Right: Time dependence of magnitudes of molecular displacements (blue solid lines) and oscillations of reflectivity changes (red solid lines). Green arrows indicate changes in molecular displacements in hypothetical equilibrium states just after photoexcitation.

coincides with the folded profile of an ω_1 oscillator expressed by $-\cos(\omega_1 t + \phi_1)$. This oscillation contains not only a $2\omega_1$ component but also higher harmonic components with $4\omega_1$, $6\omega_1$, and so on. When we focus on the $4\omega_1$ components in the Fourier power spectra at 0.5 ps [Fig. 3(b)], we notice that the spectral weight in the $4\omega_1 (=186 \text{ cm}^{-1})$ region is considerably enhanced above 0.02 ph/TCNQ, where the 93 cm^{-1} mode gains in intensity. This also supports our interpretation that the dimerization is completely melted at large x_{ph} , and the magnitude of the dimerization oscillates as the folded mode [Fig. 4(b)(iv)], as shown by the purple solid line $[-\cos(\omega_1 t + \phi_1)]$ in Fig. 2(d).

The important factor determining photoinduced incomplete or complete melting of the spin-Peierls phase is the interchain interaction, which orders the dimerization three-dimensionally. Below 0.02 ph/TCNQ, where the melted regions are not very large, the Fourier power spectra do not change greatly [Fig. 3(b)], and the spectral intensities increase linearly [Fig. 3(c)]. In such cases, a photoexcited chain is surrounded by stable dimerized chains [Fig. 4(a)]. The interchain interaction between neighboring TCNQ stacks should preserve the dimerization in the photoexcited chain and prevent complete release of the dimerization. This correlation between the dimerization phases of neighboring TCNQ stacks is expected to occur through an octahedral structure consisting of six N atoms of TCNQ surrounding a Na ion [Fig. 1(c)]. This causes the ω_1 oscillation of the reflectivity. When x_{ph} is increased and the spin-Peierls phase is destabilized in almost the entire region of a crystal [Fig. 4(b)], this interchain interaction cannot work, but the dimerization can completely disappear. This is why the $2\omega_1$ oscillation is observed.

Finally, we discuss the temporal evolution of the dimeric molecular displacements. The $2\omega_1$ oscillation component

disappears at ~ 1 ps, and after 1 ps, the ω_1 oscillation component appears, indicating that the dimerization recovers. This time is reasonably related to the photocarrier decay time of ~ 1.8 ps [33], as mentioned above. Thus, we can summarize the overall photocarrier dynamics as follows: under strong photoirradiation, photocarriers are generated so densely that the spin-Peierls phase is three-dimensionally destabilized, producing the $2\omega_1$ oscillation [Fig. 4(b)]. When photocarriers recombine and their number decreases, dimeric molecular displacements are restored and the ω_1 oscillation is observed.

IV. SUMMARY

We investigated photoinduced melting of the spin-Peierls phase in Na-TCNQ by PP reflection spectroscopy with a time resolution of 49 fs. The doubling of the coherent oscillation frequency of the transient reflectivity was observed under strong photoexcitation of the spin-Peierls phase. This frequency conversion was reasonably attributed to the complete melting of the spin-Peierls phase, which originates in three-dimensional destabilization of the dimerization. This is an observation of the photoinduced recovery of an original symmetry revealed by frequency doubling of coherent oscillation. This frequency doubling is expected to be detected in various types of photoinduced phase transitions from low-symmetry to high-symmetry phases and should be direct evidence of complete recovery of the original symmetry.

ACKNOWLEDGMENTS

This work was supported in part by a Grant-in-Aid from the Japan Society for the Promotion of Science (JSPS) (Grant No. 25247049).

-
- [1] For a review, see *Photoinduced Phase Transitions*, edited by K. Nasu (World Scientific, Singapore, 2004).
- [2] S. Iwai and H. Okamoto, *J. Phys. Soc. Jpn.* **75**, 011007 (2006).
- [3] S. Iwai, M. Ono, A. Maeda, H. Matsuzaki, H. Kishida, H. Okamoto, and Y. Tokura, *Phys. Rev. Lett.* **91**, 057401 (2003).
- [4] H. Okamoto, H. Matsuzaki, T. Wakabayashi, Y. Takahashi, and T. Hasegawa, *Phys. Rev. Lett.* **98**, 037401 (2007).
- [5] H. Okamoto, T. Miyagoe, K. Kobayashi, H. Uemura, H. Nishioka, H. Matsuzaki, A. Sawa, and Y. Tokura, *Phys. Rev. B* **83**, 125102 (2011).
- [6] A. Cavalleri, C. Tóth, C. W. Siders, J. A. Squier, F. Raksi, P. Forget, and J. C. Kieffer, *Phys. Rev. Lett.* **87**, 237401 (2001).
- [7] A. Cavalleri, M. Rini, H. H. W. Chong, S. Fourmaux, T. E. Glover, P. A. Heimann, J. C. Kieffer, and R. W. Schoenlein, *Phys. Rev. Lett.* **95**, 067405 (2005).
- [8] C. Kübler, H. Ehrke, R. Huber, R. Lopez, A. Halabica, R. F. Haglund, Jr., and A. Leitenstorfer, *Phys. Rev. Lett.* **99**, 116401 (2007).
- [9] P. Baum, D.-S. Yang, and A. H. Zewail, *Science* **318**, 788 (2007).
- [10] S. Wall, D. Wegkamp, L. Foglia, K. Appavoo, J. Nag, R. F. Haglund, Jr., J. Stähler, and M. Wolf, *Nat. Commun.* **3**, 721 (2012).
- [11] M. Fiebig, K. Miyano, Y. Tomioka, and Y. Tokura, *Science* **280**, 1925 (1998).
- [12] M. Fiebig, K. Miyano, Y. Tomioka, and Y. Tokura, *Appl. Phys. B* **71**, 211 (2000).
- [13] M. Rini, R. Tobey, N. Dean, J. Itatani, Y. Tomioka, Y. Tokura, R. W. Schoenlein, and A. Cavalleri, *Nature* **449**, 72 (2007).
- [14] M. Matsubara, Y. Okimoto, T. Ogasawara, Y. Tomioka, H. Okamoto, and Y. Tokura, *Phys. Rev. Lett.* **99**, 207401 (2007).
- [15] Y. Okimoto, H. Matsuzaki, Y. Tomioka, I. Kezsmarki, T. Ogasawara, M. Matsubara, H. Okamoto, and Y. Tokura, *J. Phys. Soc. Jpn.* **76**, 043702 (2007).
- [16] D. Polli, M. Rini, S. Wall, R. W. Schoenlein, Y. Tomioka, Y. Tokura, G. Cerullo, and A. Cavalleri, *Nat. Mater.* **6**, 643 (2008).
- [17] M. Chollet, L. Guerin, N. Uchida, S. Fukaya, H. Shimoda, T. Ishikawa, K. Matsuda, T. Hasegawa, A. Ota, H. Yamochi, G. Saito, R. Tazaki, A. Adachi, and S. Koshihara, *Science* **307**, 86 (2005).
- [18] S. Iwai, K. Yamamoto, A. Kashiwazaki, F. Hiramatsu, H. Nakaya, Y. Kawakami, K. Yakushi, H. Okamoto, H. Mori, and Y. Nishio, *Phys. Rev. Lett.* **98**, 097402 (2007).
- [19] S. Koshihara, Y. Tokura, T. Mitani, G. Saito, and T. Koda, *Phys. Rev. B* **42**, 6853 (1990).
- [20] E. Collet, M. H. Cailleau, M. B. Cointe, H. Cailleau, M. Wulff, T. Luty, S. Koshihara, M. Meyer, L. Toupet, P. Rabiller, and S. Techert, *Science* **300**, 612 (2003).

- [21] H. Okamoto, Y. Ishige, S. Tanaka, H. Kishida, S. Iwai, and Y. Tokura, *Phys. Rev. B* **70**, 165202 (2004).
- [22] S. Iwai, Y. Ishige, S. Tanaka, Y. Okimoto, Y. Tokura, and H. Okamoto, *Phys. Rev. Lett.* **96**, 057403 (2006).
- [23] L. Guérin, J. Hébert, M. Buron-Le Cointe, S.-i. Adachi, S.-y. Koshihara, H. Cailleau, and E. Collet, *Phys. Rev. Lett.* **105**, 246101 (2010).
- [24] H. Uemura and H. Okamoto, *Phys. Rev. Lett.* **105**, 258302 (2010).
- [25] T. Miyamoto, K. Kimura, T. Hamamoto, H. Uemura, H. Yada, H. Matsuzaki, S. Horiuchi, and H. Okamoto, *Phys. Rev. Lett.* **111**, 187801 (2013).
- [26] L. Perfetti, P. A. Loukakos, M. Lisowski, U. Bovensiepen, H. Berger, S. Biermann, P. S. Cornaglia, A. Georges, and M. Wolf, *Phys. Rev. Lett.* **97**, 067402 (2006).
- [27] F. Schmitt, P. S. Kirchmann, U. Bovensiepen, R. G. Moore, L. Rettig, M. Krenz, J. H. Chu, N. Ru, L. Perfetti, D. H. Lu, M. Wolf, I. R. Fisher, and Z. X. Shen, *Science* **321**, 1649 (2008).
- [28] R. Yusupov, T. Mertelj, V. V. Kabanov, S. Brazovskii, P. Kusar, J. Chu, I. R. Fisher, and D. Mihailovic, *Nat. Phys.* **6**, 681 (2010).
- [29] A. Tomeljak, H. Schäfer, D. Städter, M. Beyer, K. Biljakovic, and J. Demsar, *Phys. Rev. Lett.* **102**, 066404 (2009).
- [30] S. Koshihara, Y. Tokura, Y. Iwasa, and T. Koda, *Phys. Rev. B* **44**, 431 (1991).
- [31] H. Okamoto, K. Ikegami, T. Wakabayashi, Y. Ishige, J. Togo, H. Kishida, and H. Matsuzaki, *Phys. Rev. Lett.* **96**, 037405 (2006).
- [32] H. Uemura, N. Maeshima, K. Yonemitsu, and H. Okamoto, *Phys. Rev. B* **85**, 125112 (2012).
- [33] K. Ikegami, K. Ono, J. Togo, T. Wakabayashi, Y. Ishige, H. Matsuzaki, H. Kishida, and H. Okamoto, *Phys. Rev. B* **76**, 085106 (2007).
- [34] M. Konno and Y. Saito, *Acta Crystallogr. Sect. B* **30**, 1294 (1974).
- [35] M. Konno and Y. Saito, *Acta Crystallogr. Sect. B* **31**, 2007 (1975).
- [36] J. W. Bray, L. V. Interrante, I. S. Jacobs, and J. S. Miller, in *Extended Linear Chain Compounds*, edited by J. S. Miller (Plenum Press, New York, 1983), Vol. 3, p. 353.
- [37] H. Terauchi, *Phys. Rev. B* **17**, 2446 (1978).
- [38] Y. Takaoka and K. Motizuki, *J. Phys. Soc. Jpn.* **47**, 1752 (1979).
- [39] Y. Lepine, *Phys. Rev. B* **28**, 2659 (1983).
- [40] H. J. Zeiger, J. Vidal, T. K. Cheng, E. P. Ippen, G. Dresselhaus, and M. S. Dresselhaus, *Phys. Rev. B* **45**, 768 (1992).
- [41] To reproduce the experimental time profile (open circles), we calculated the convolution integrals of the curve $[-|\cos(\omega_1 t + \phi_1)|]$ with the term $[\exp(-t^2/\tau_0^2)]$ corresponding to a time resolution of 49 fs.
- [42] For the red line in Fig. 2(d), we used the same values of ω_1 and τ_1 as used for the red line in Fig. 2(c).
- [43] H. Suzuki, T. Kinjo, Y. Hayashi, M. Takemoto, and K. Ono, *J. Acoust. Emiss.* **14**, 69 (1996).